

SOUS VIDE: Cooking Visual Drone Navigation Policies in a Gaussian Splatting Vacuum

JunEn Low¹, Maximilian Adang², Javier Yu², Keiko Nagami², and Mac Schwager²

Abstract—We propose a new simulator, training approach, and policy architecture, collectively called SOUS VIDE, for end-to-end visual drone navigation. Our trained policies exhibit zero-shot sim-to-real transfer with robust real-world performance using only on-board perception and computation. Our simulator, called FiGS, couples a computationally simple drone dynamics model with a high visual fidelity Gaussian Splatting scene reconstruction. FiGS can quickly simulate drone flights producing photorealistic images at up to 130 fps. We use FiGS to collect 100k-300k observation-action pairs from an expert MPC with privileged state and dynamics information, randomized over dynamics parameters and spatial disturbances. We then distill this expert MPC into an end-to-end visuomotor policy with a lightweight neural architecture, called SV-Net. SV-Net processes color image, optical flow and IMU data streams into low-level body rate and thrust commands at 20Hz onboard a drone. Crucially, SV-Net includes a Rapid Motor Adaptation (RMA) module that adapts at runtime to variations in drone dynamics. In a campaign of 105 hardware experiments, we show SOUS VIDE policies to be robust to 30% mass variations, 40 m/s wind gusts, 60% changes in ambient brightness, shifting or removing objects from the scene, and people moving aggressively through the drone’s visual field. Code, data, and experiment videos can be found on our project page: <https://stanfordml.github.io/SousVide/>.

I. INTRODUCTION

LEARNED visuomotor policies offer a compelling alternative to traditional drone navigation stacks by unifying perception and control into a streamlined framework. Unfortunately, training policies with human-like agility and collision avoidance requires a large corpus of visual and state data, making behavior cloning from human pilot demonstrations impractical. Simulation provides a promising alternative, but the sim-to-real gap has remained a persistent obstacle to real-world deployment. When overcome, these policies have shown highly agile, superhuman performance [1]–[3]. However, such successes are limited to racing tracks designed for easy simulation reconstruction or hand-crafted simulation environments built from graphics asset libraries. This raises the question: how can we train an agile visuomotor policy to navigate cluttered real-world environments without relying on human input?

We address this challenge with FiGS (Flying in Gaussian Splats), a photorealistic drone simulator combining a Gaussian Splatting (GSplat) [4] scene model with a lightweight 9-dimensional drone dynamics model using thrust and body rate

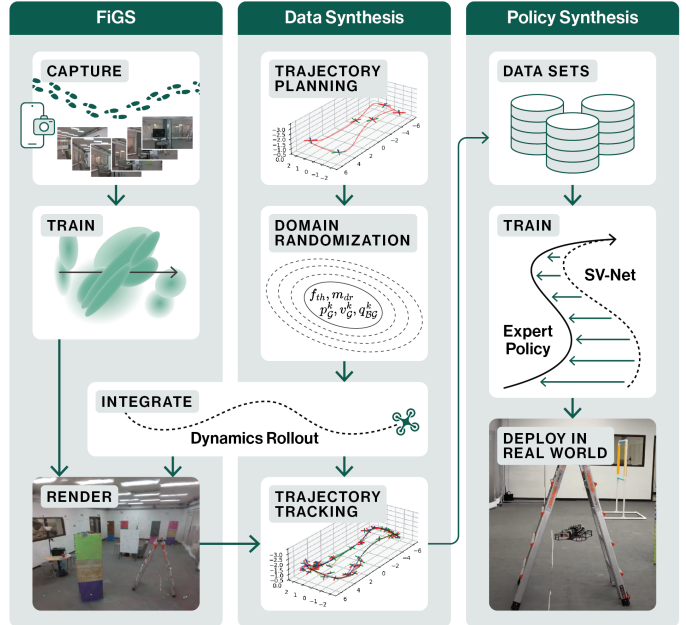


Fig. 1. SOUS VIDE: Our simulator, FiGS, combines a GSplat scene model with a lightweight drone dynamics model. Within FiGS, an MPC policy generates demonstrations that track a desired trajectory across randomized drone dynamics and spatial disturbances. These are used to train a visuomotor policy, SV-Net, that we deploy zero-shot in the real-world.

inputs—equivalent to the Acro mode used by expert human pilots. FiGS reconstructs scenes from handheld video captures with standard tools [5] and generates realistic image sequences and state estimation data for a drone at over 100 fps, all within an hour of acquiring video data on a standard GPU. This contrasts with the current practice of approximating each real scene with a handcrafted simulation instance [6]–[11] that can take weeks of laborious sim-to-real transfer to perfect.

Building on FiGS, we develop a complete behavior cloning policy training pipeline and policy architecture for drone navigation, shown in Fig. 1. We call the combined simulator, training pipeline, and policy SOUS VIDE (Scene Optimized Understanding via Synthesized Visual Inertial Data from Experts). With SOUS VIDE, we can train a visuomotor policy to robustly navigate a drone in a real environment zero-shot—the policy has no access to real flight data at training time. Indeed, we can train policies to navigate drones through environments that neither the drone nor the users have previously visited, using remotely captured video or publicly available recordings.

Specifically, we use FiGS to generate 100k-300k image/state-action pairs from an expert MPC policy following a desired nominal trajectory. The MPC has access to the ground truth state in the simulator and is therefore able to demonstrate high-quality, collision-free trajectories. To obtain stable and robust flight, we randomize dynamics parameters

*This work was supported in part by DARPA grant HR001120C0107, ONR grant N00014-23-1-2354, and Lincoln Labs grant 7000603941. The second author was supported on an NDSEG fellowship. Toyota Research Institute provided funds to support this work.

¹Department of Mechanical Engineering, Stanford University, Stanford, CA 94404, USA jelow@stanford.edu

²Department of Aeronautics and Astronautics, Stanford University, Stanford, CA 94404, USA {madang, javieryu, knagami, schwager}@stanford.edu

and spatial perturbations and record the MPC’s response. We use these expert demonstrations to train a student policy without privileged information (e.g. no lateral position data).

For the student policy, we introduce a new architecture, called SV-Net, that is rich enough to ingest image and observable state history, while being efficient enough to run at 20Hz on board the drone. The policy ingests images using a SqueezeNet [12], re-trained on our data, and outputs a feature vector that is fused with observable data across several small MLPs to produce control commands. Within these, we also implement a form of the Rapid Motor Adaptation (RMA) concept from [13], which takes a history of observable data from a sliding window and produces a latent code that captures evolving flight dynamics in real time. We find this RMA module is crucial for robust real-world flight, adapting online to variations such as battery drain, rotor downwash effects and wind gusts.

To summarize, we introduce SOUS VIDE, which incorporates the following contributions:

- 1) **Flying in Gaussian Splats (FiGS):** A simulator coupling GSplat scene models with lightweight drone dynamics for photorealistic visual-inertial flight data.
- 2) **Expert Demonstration Data:** We use an MPC expert to synthesize behavior cloning data in FiGS with randomized dynamics parameters and positional disturbances.
- 3) **SV-Net:** A robust, efficient policy combining image and observable data to infer thrust and body rates, with RMA enabling online adaptation to changing flight conditions.

We evaluate SOUS VIDE policies across 105 hardware flights in 4 different scenes, testing 9 different experimental conditions. We demonstrate our policy’s robustness to 30% mass variations, 40 m/s wind gusts, 60% changes in ambient brightness, shifting or removing objects from the scene, and people moving aggressively through the drone’s visual field.

The paper is organized as follows: Section II reviews related work, Section III describes the FiGS simulator, Section IV details the MPC-based data synthesis, and Section V presents the SV-Net policy. Hardware experiments are in Section VI, with conclusions, limitations, and future work in Section VII.

II. RELATED WORK

Drone Policies Trained with GSplats: We are inspired by the recent works [14], [15] that train drone policies with visual data from a GSplat or Neural Radiance Field (NeRF) scene model. Most similar to our method, [14] uses a NeRF and an MPC expert to train a policy for trajectory following, but is not zero-shot (it requires real flight data) and it does not navigate through cluttered scenes. A zero-shot policy trained in a GSplat is presented in [15], but it is limited to tracking pre-placed visual markers with high-level commands that do not react to the obstacles in the scene. Some works have used GSplats for manipulation [16], [17], and locomotion [18] policies, but they are not applied to drone flight. To the best of our knowledge, SOUS VIDE is the first method to use GSplats to produce zero-shot drone navigation policies.

Training Drone Policies in Simulation: Simulators offer scalability and safety in collecting training data, but they introduce a sim-to-real gap, making it difficult to transfer policies to

the real world. Many existing works use domain randomization [19] to robustify policies, as we also do. For drones, another common strategy is to enhance the fidelity of the drone dynamics model with drag and other effects [20]–[22], while another is to improve rendering pipelines and graphics assets [6]–[11]. However, none of these approaches can match the speed and visual fidelity of GSplat scene reconstructions. Another prevalent solution involves visual abstractions, such as depth maps [1], [23] or learned feature embeddings [2], which aim to distill visual information into a domain-invariant representation. However, this discards information encoded in raw pixel data that could otherwise improve task performance.

High-performance simulation-trained policies have been demonstrated for drone racing [1]–[3], marking an impressive technological achievement. However, these methods blend real and simulation flight data, physics and learning-based models, and hand-engineered visual features cued into racing gates. In contrast, our method can train a policy using a casual video capture of any environment and can transfer zero-shot to the real-world scene without hand-tuned features.

Rapid Motor Adaptation (RMA): We borrow the concept of Rapid Motor Adaptation, originally developed for quadruped locomotion policies in [13]. RMA can be viewed as a pre-trained alternative to online parameter estimation [24]. RMA trains an encoder from sensing history to a latent vector that captures runtime operating conditions (e.g., terrain for a quadruped, or flight dynamics for a drone). RMA has been adapted for drones in [25], [26]. These policies achieve stable flight with impressive robustness but are not designed for visual navigation. Our lightweight RMA implementation is crucial for real-world robustness, addressing variations in both modeled and unmodeled drone dynamics.

Generalist Collision Avoidance Policies: Some existing works train policies to steer a drone through environments not seen at training time, often focusing on a particular scene domain like forests [27], office buildings [28], or urban roadways [29]. Such policies have been trained both with RL [28] and with imitation learning [27], [29], using both simulated [23], [28] and real-world [27], [30]–[32] data. Recent examples strive toward policies that can operate across different robot embodiments [31], [32]. While impressive for their generality, they often treat the drone as a pseudo-static ground robot by using a finely tuned onboard Visual-Inertial Odometry (VIO) stack to constrain the dynamics to planar velocities and yaw. This fails to exploit the drone’s full agility when navigating cluttered indoor environments with complex 3D trajectories. In contrast, SOUS VIDE directly commands thrust and body rates, mirroring the capabilities of expert human pilots.

III. FLYING IN GAUSSIAN SPLATS (FiGS)

Here we describe the main components of our lightweight GSplat-based flight simulator, FiGS. We first collect a sequence of environment training images and train a GSplat model. We then forward integrate a simplified 9-dimensional drone dynamics model and render images from the GSplat as viewed through the onboard camera.

Gaussian Splats: 3D Gaussian Splats [4] represent a 3D scene with a large collection of 3D Gaussians (up to millions),

parameterized by mean $\mu \in \mathbf{R}^3$, covariance matrix $\Sigma \in \mathbf{S}_{++}$, opacity $\alpha \in [0, 1]$, and spherical harmonics for view-dependent color, to approximate the geometry and appearance of real-world scenes. GSplats are coupled with a high-speed projection-based differentiable image rendering method called rasterization. They are trained from a sparse set of RGB images by backpropagating through the rasterization rendering to minimize photometric error between rendered images and training images. This approach achieves photorealistic reconstructions and renders full-resolution images at over 100 fps on a standard desktop GPU.

In this work, we generate GSplats from short video recordings (1-2 minutes) of scene walk-throughs with a handheld camera. From the video we obtain a set of training images $(\mathcal{I}_0^{gt}, \dots, \mathcal{I}_N^{gt})$ and train the GSplat with the standard open-source tool Nerfstudio [5], [33]. The trained GSplat, $\mathcal{I} = \text{GS}_\phi(\mathbf{p}, \mathbf{q})$, parametrized by ϕ , can render photorealistic images \mathcal{I} from a virtual camera placed at any pose (translation and quaternion rotation (\mathbf{p}, \mathbf{q})) in the scene within the area covered by the training images. We obtain metric scale and align the GSplat frame to a known global frame in the scene by placing an ArUco tag marker on the ground during training.

Drone Dynamics Model: Our model operates in the world, body, and camera frames $(\mathcal{W}, \mathcal{B}, \mathcal{C})$ and uses a simplified 9-dimensional semi-kinematic drone model. The states $\mathbf{x} = [\mathbf{p}_{\mathcal{W}} \ \mathbf{v}_{\mathcal{W}} \ \mathbf{q}_{\mathcal{B}\mathcal{W}}]^T$, represent translation ($\mathbf{p}_{\mathcal{W}}$), velocity ($\mathbf{v}_{\mathcal{W}}$) and quaternion orientation ($\mathbf{q}_{\mathcal{B}\mathcal{W}}$). The control inputs $\mathbf{u} = [f_{th} \ \boldsymbol{\omega}_{\mathcal{B}}]^T$ include normalized thrust (f_{th}) and desired angular velocities ($\boldsymbol{\omega}_{\mathcal{B}}$), forming the dynamics model

$$\begin{aligned} \dot{\mathbf{p}}_{\mathcal{W}} &= \mathbf{v}_{\mathcal{W}}, \\ \dot{\mathbf{v}}_{\mathcal{W}} &= -g\mathbf{z}_{\mathcal{W}} + k_{th} \frac{\hat{f}_{th}}{m_{dr}} \mathbf{z}_{\mathcal{B}}, \\ \dot{\mathbf{q}}_{\mathcal{B}\mathcal{W}} &= \frac{1}{2} \mathbf{W}(\boldsymbol{\omega}_{\mathcal{B}}) \mathbf{q}_{\mathcal{B}\mathcal{W}}, \end{aligned} \quad (1)$$

where g is gravitational acceleration, $\mathbf{W}(\boldsymbol{\omega}_{\mathcal{B}})$ is the quaternion multiplication matrix, and $\mathbf{z}_{\mathcal{W}}$ and $\mathbf{z}_{\mathcal{B}}$ are the world frame and body frame z-axis respectively. The model parameters $\boldsymbol{\theta} = [k_{th} \ m_{dr}]$ represent the thrust coefficient and drone mass.

Body rate commands are the standard low-level input for most flight controllers [1]–[3], [21], providing robust tracking through high-rate gyroscope feedback. This choice also enhances platform agnosticism in a cost-effective manner and is widely favored by expert human pilots. Moreover, for our specific use case, it offers the significant advantage of omitting the rotational acceleration equations (Euler’s equations) in (1).

We forward integrate these equations of motion using ACADOS [34], a highly efficient trajectory optimizer that provides direct access to its integrator, to obtain state and control trajectories $(\mathbf{u}_{0:N-1}, \mathbf{x}_{0:N})$. Applying a body-camera transform, we can render an image sequence from the GSplat $\mathcal{I}_{0:N}$ as seen by the onboard camera to yield data for policy training. This data can be used in a Reinforcement Learning (RL) or Imitation Learning (IL) framework, and can supervise training of either state-feedback or image-feedback policies. For SOUS VIDE, we use an IL framework with an MPC expert from ACADOS, which we will describe next.

IV. MPC EXPERT AND DATA SYNTHESIS

SOUS VIDE generates visuomotor policies in two steps. First, it programmatically synthesizes a large dataset of demonstrations from an MPC expert policy with privileged state information using our simulator, FiGS. Then, it distills these demonstrations into a policy deployed on the drone.

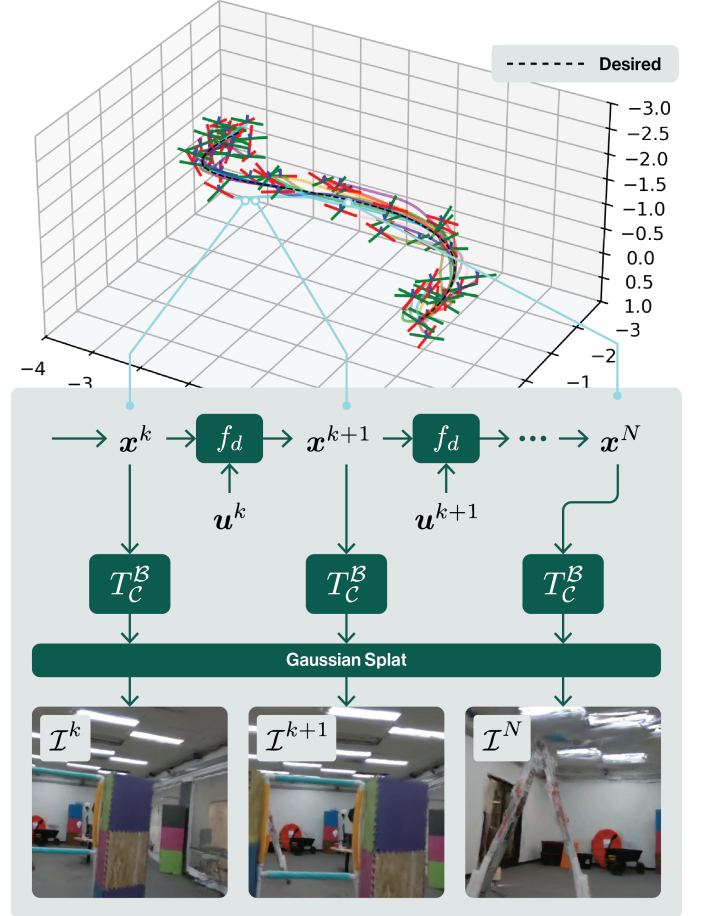


Fig. 2. Dynamic rollout of 50 data samples. At each time step, the update equation f_d simulates the solution from the MPC expert, while the transform T_C^B is used to extract the corresponding camera image \mathcal{I} from the GSplat.

We begin by generating a desired trajectory through solving the minimum snap trajectory problem outlined in [35], which takes a sequence of position-yaw waypoints and outputs a dynamically feasible spline, from which a state trajectory and open-loop control trajectory are obtained through the differential flatness map. This waypoint-based approach allows us to interface with various high-level planners commonly used in drone trajectory planning. By sampling at our policy’s control frequency, ν_{ctl} , we produce a N_{des} step trajectory $\mathbf{X}^{des} = \{\mathbf{x}_0^{des}, \dots, \mathbf{x}_{N_{des}}^{des}\}$ with control inputs parametrized by the drone dynamics parameters $\boldsymbol{\theta}$, $\mathbf{U}^{des} = \{\mathbf{u}_0^{des}, \dots, \mathbf{u}_{N_{des}-1}^{des}\}$.

A large demonstration dataset can be generated using any trajectory optimization technique with dynamics rollouts, such as the one-shot sampling methods in [36] or by iteratively running DAGger [37] in simulation. We opt for the simplest approach, domain randomization, as described in Algo. IV and illustrated in Fig. 2. This leverages the strength of FiGS in quickly producing large volumes of photorealistic image data while leaving the door open to more sophisticated techniques.

We define $(\theta_{\min}, \theta_{\max}, \Delta\mathbf{x})$ as the bounds on the uniform distributions on the drone parameters and sample states, N_{smp} is the step-wise sample count and \mathcal{GS} is the Gaussian Splat. We observe that these bounds can be liberally set. `GenerateDynamics` instantiates (1) with a given set of drone parameters (f_d in Fig. 2), `GenerateImage` extracts the camera pose given the drone state and camera transform (T_C^B in Fig. 2) before rendering the corresponding image from the Gaussian Splat (\mathcal{I}^k in Fig. 2). `TMPC` is our expert policy that uses MPC to track X^{des} and U^{des} , starting from the nearest position to \mathbf{x}_s for t_{smp} seconds. We optimize

$$\begin{aligned} \min_{\mathbf{u}} \sum_{k=0}^{N-1} (\delta\mathbf{x}_k^T Q_k \delta\mathbf{x}_k + \delta\mathbf{u}_k^T R_k \delta\mathbf{u}_k) + \delta\mathbf{x}_N^T Q_N \delta\mathbf{x}_N \quad (2) \\ \text{s.t. } \mathbf{x}_{k+1} = f_d(\mathbf{x}_k, \mathbf{u}_k), \quad g_c(\mathbf{u}_k) \leq \mathbf{0} \end{aligned}$$

in an N -step receding horizon manner, subject to dynamics constraint f_d and the control limits constraint g_c . The stage-wise weights, (Q_k, R_k) , and the terminal weights, Q_N , are applied to the difference between the rollout trajectory and the desired trajectory, defined $\delta\mathbf{x}_k = (\mathbf{x}_k - \mathbf{x}_k^{\text{des}})$, and similarly for $\delta\mathbf{u}_k$. We use ACADOS to implement the MPC using it, though alternative solvers could be employed.

Algorithm 1 FiGS Domain Randomization

Require: $\mathbf{X}^{\text{des}}, \mathbf{U}^{\text{des}}, \theta_{\min}, \theta_{\max}, \Delta\mathbf{x}, N_{\text{des}}, N_{\text{smp}}, t_{\text{smp}}, T_C^B, \mathcal{GS}$

- 1: Initialize dataset $\mathcal{D} = \emptyset$
- 2: **for** $i = 0$ to $N_{\text{des}} - 1$ **do**
- 3: **for** $j = 0$ to N_{smp} **do**
- 4: $\theta_s \sim U(\theta_{\min}, \theta_{\max}), \mathbf{x}_s \sim (\mathbf{x}_i^{\text{des}} - \Delta\mathbf{x}, \mathbf{x}_i^{\text{des}} + \Delta\mathbf{x})$
- 5: $f_d \leftarrow \text{GenerateDynamics}(\theta_s)$
- 6: $\mathbf{X}^{\text{smp}}, \mathbf{U}^{\text{smp}} = \text{TMPC}(\mathbf{x}_s, f_d, t_{\text{smp}}, \mathbf{X}^{\text{des}}, \mathbf{U}^{\text{des}})$
- 7: $\mathbf{I}^{\text{smp}} = \text{GenerateImage}(\mathbf{X}^{\text{smp}}, T_C^B, \mathcal{GS})$
- 8: $\mathcal{D} \leftarrow \mathcal{D} \cup \{(\mathbf{X}^{\text{smp}}, \mathbf{U}^{\text{smp}}, \mathbf{I}^{\text{smp}})\}$

V. SV-NET POLICY ARCHITECTURE

Our policy architecture, SV-Net, runs on an Orin Nano onboard the drone at 20 Hz and is illustrated in Fig. 3. The policy relies exclusively on data directly observable by the drone: (i) images from the onboard camera and (ii) state estimates of vertical position, translational velocities, and quaternion orientation $(p_{z\mathcal{W}}^k, \mathbf{v}_{\mathcal{W}}^k, \mathbf{q}_{B\mathcal{W}}^k)$, derived from an EKF. These estimates are typically obtained on a drone by fusing data from an IMU, a downward-facing time-of-flight sensor, and an optical flow sensor—all of which are mature, small-footprint, and plug-and-play units commonly available on hobby-grade drones. The policy outputs thrust and body rate commands $\mathbf{u}^k = (f_{th}, \boldsymbol{\omega})$, a standard control mode used by FPV drone racing pilots.

SV-Net comprises three components: a feature extractor, a history network and a command network. The architecture uses SqueezeNet [12] as a vision encoder, augmenting its output with estimated height and orientation before passing it through an MLP to create a pose-aware feature extractor. The history network uses a sliding T-step window of the observable state to generate a latent vector encoding the evolving flight dynamics of the drone at that instant, a technique

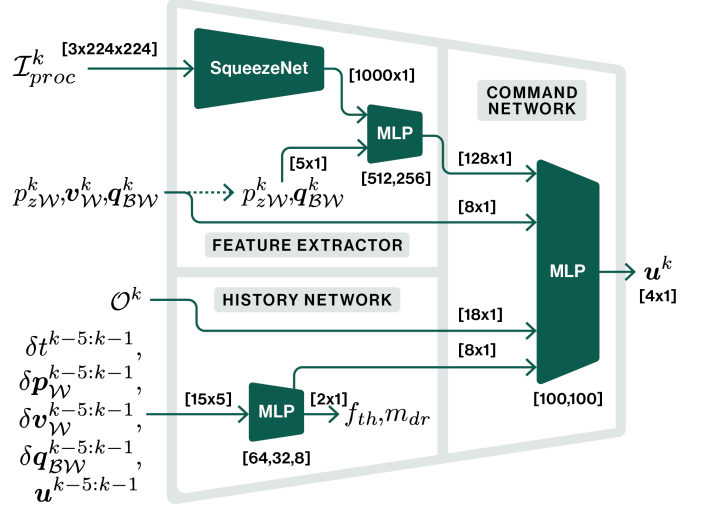


Fig. 3. SV-Net consists of three components: a feature extractor that processes visual information from color images, a history network that uses an RMA technique to adapt to variations in dynamics through a history of observable states, and a command network that integrates the outputs of these components with observable states to generate body-rate commands.

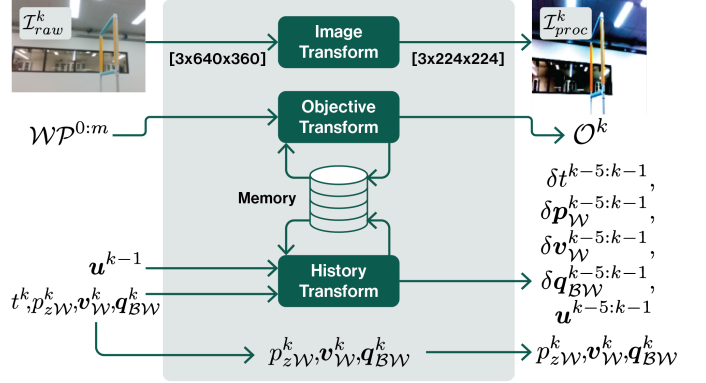


Fig. 4. The data pre-processing step used in SV-Net policy. The blue hue of the processed image, \mathcal{I}_{proc}^k , illustrates the color normalization in contrast to the raw image, \mathcal{I}_{raw}^k , with both displayed using a $[0, 1]$ visualization range.

called Rapid Motor Adaptation (RMA). The policy ingests the latent vector to adapt its output to current flight conditions. The command network combines the outputs of the feature extractor and history network with the observable states and a user-defined objective \mathcal{O}^k . This objective encodes the first and last waypoints of the trajectory and the total trajectory time. This remains constant at deployment except for when we use a single policy to encode multiple trajectories. The policy inputs are derived from onboard sensor data using the pre-processing outlined in Fig. 4, where raw images are scaled and normalized, and observable EKF data is processed through the history transform defined by:

$$\begin{aligned} \delta t^{k-1} &= t^k - t^{k-1} \\ \delta p_{\mathcal{W}}^{k-1} &= \delta t^{k-1} \cdot \mathbf{v}^k \\ \delta \mathbf{v}_{\mathcal{W}}^{k-1} &= \mathbf{v}^k - \mathbf{v}^{k-1} \\ \delta \mathbf{q}_{B\mathcal{W}}^{k-1} &= \mathbf{q}_{\mathcal{W}B}^k \cdot \mathbf{q}_{B\mathcal{W}}^{k-1}. \end{aligned} \quad (3)$$

Note that we use velocity to back out a change in position for the RMA module. We do not use positional information from VIO or external motion capture for this.

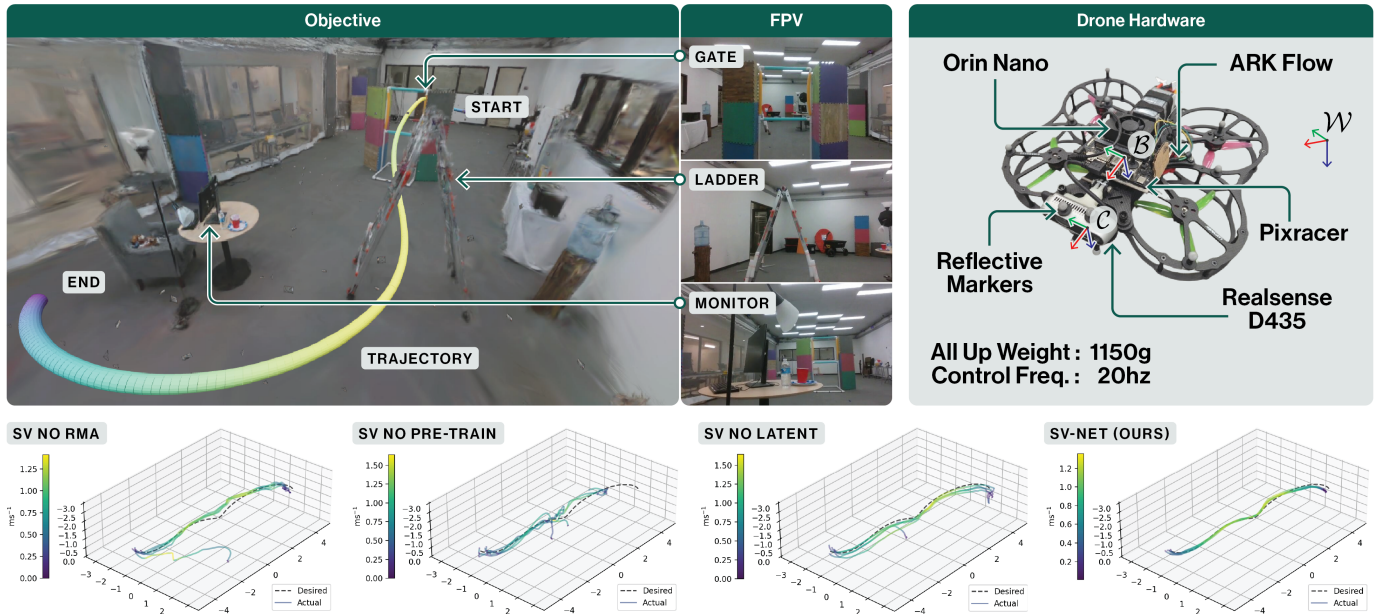


Fig. 5. Clockwise from top left: 1) Flight test objectives shown as a 3D projection onto the Gaussian Splat and in real-world FPV. 2) Drone hardware setup with frames (\mathcal{W} , \mathcal{B} , \mathcal{C}). We use a PixRacer Pro for low-level control and an Orin Nano for policy execution. Sensing is done using the PixRacer’s IMU, an ARK Flow sensor, motion capture markers and the D435’s monocular camera. 3) 3D plots depicting real-world performance of the policies in Section VI-A.

To train the policy, we first pre-train the RMA network on the sampled drone parameters. Once trained, the RMA network is frozen, and the remaining components of the policy are trained end-to-end (including the SqueezeNet image encoder) to predict body rate commands. In hardware testing, we find the best performance is achieved using the output of the second-to-last layer, not the explicit estimate of θ , as input into the command network MLP.

A. Analysis of RMA Module

A property of (1) is that if we allow the drone parameters, k_{th} and m , to be variables that can be adjusted online, we can use them to compensate for a wide range of model inaccuracies that are not limited to the thrust and weight of the drone. For simplicity, let $c = \frac{k_{th}}{m}$. Given an additional force vector \mathbf{f}_{add} in the world frame to account for model inaccuracies from the thrust coefficient, mass and also for any external forces like aerodynamic drag or ground effect, we can compute an equivalent \hat{c} in an augmented form of the velocity equation in (1). We start by doing

$$-gz_{\mathcal{W}} + \hat{c}f_{th}z_{\mathcal{B}} = -gz_{\mathcal{W}} + cf_{th}z_{\mathcal{B}} + \mathbf{f}_{add} \quad (4)$$

and then taking the least-squares estimate of \hat{c} , we get:

$$\hat{c} \approx \frac{c + z_{\mathcal{B}}^T \mathbf{f}_{add}}{\hat{f}_{th}}. \quad (5)$$

As evidenced in (5), the capacity of \hat{c} to accurately approximate additional forces hinges on near-collinearity of $z_{\mathcal{B}}$ and \mathbf{f}_{add} . This constraint is acceptable for most drone applications. For instance: (i) by definition, thrust-related additional forces align with the $z_{\mathcal{B}}$ axis, (ii) much of the drone’s operational envelope is near-hover, where $z_{\mathcal{B}}$ aligns closely with primarily vertical forces, such as those due to changes in mass and ground effect, and (iii) at higher speeds, aerodynamic drag aligns with $z_{\mathcal{B}}$, as the motor thrust vector must follow the flight

direction. Hence, the RMA module can account for variations in flight dynamics the drone encounters during flight.

VI. EXPERIMENTS

In this section, we evaluate our SOUS VIDE policies across three fronts: efficacy of the proposed policy architecture, robustness to dynamic and visual disturbances, and generalization to novel scenarios. We demonstrate that the SV-Net policy, equipped with the RMA module, achieves state-of-the-art performance in zero-shot sim-to-real transfer. We emphasize that in all our experiments, the policy does not get to observe lateral position ($p_{x\mathcal{W}}, p_{y\mathcal{W}}$), e.g., from a motion capture system, or an onboard VIO system. We do obtain vertical position $p_{z\mathcal{W}}$ from the onboard time-of-flight sensor.

We perform all experiments using a quadrotor drone equipped with a PixRacer Pro for low-level body-rate tracking control and an Orin Nano for policy execution, as shown in Fig. 5. The onboard sensing suite includes an IMU, ARK Flow sensor, and a monocular camera. The motion capture markers visible in our images and videos are for diagnostics (to plot trajectories and compare against ground truth). To assess performance, we evaluate the following metrics:

- **Success:** Completes the intended trajectory. We subdivide this into: 1) no collisions and 2) collisions that recover.
- **Partial Success:** Tracks the position, but not orientation.
- **Failure:** Fails to finish the trajectory. We subdivide this into: 1) collisions that do not recover 2) drifts off-course.
- **Collision Rate:** The number of collisions the drone makes, normalized by the total distance it traveled.
- **Trajectory Tracking Error:** The ℓ_2 -norm of the drone’s position to the nearest point on the desired trajectory.
- **Proximity Percentile:** The percentage of the actual trajectory that is within a distance $r=0.3m$ of the desired.

These metrics ensure a comprehensive evaluation of trajectory adherence, robustness, and recovery behavior.

Ablation Experiments	Success		Partial Success	Failure		Collision Rate (hits/m)	Trajectory Tracking Error (m)	Proximity Percentile (%)
	No Collisions	Recovery		No Recovery	Off-Course			
SV no RMA	3	0	1	0	1	0.00	0.646	37.7
SV no pre-train	0	0	1	4	0	0.10	0.392	51.4
SV no latent	1	2	1	1	0	0.05	0.434	42.0
SV-Net (ours)	5	0	0	0	0	0.00	0.173	96.0

TABLE I
TABLE COMPARING THE PERFORMANCE OF THE SV-NET AND ITS ARCHITECTURE ABLATIONS

Robustness Experiments	Success		Partial Success	Failure		Collision Rate (hits/m)	Trajectory Tracking Error (m)	Proximity Percentile (%)
	No Collisions	Recovery		No Recovery	Off-Course			
Baseline	5	0	0	0	0	0.00	0.173	96.0
Lighting	4	0	1	0	0	0.00	0.237	64.2
Dynamic	5	0	0	0	0	0.00	0.188	86.3
Static	0	0	4	0	1	0.06	0.488	25.3
Payload	5	0	0	0	0	0.00	0.202	80.1
Wind	5	0	0	0	0	0.00	0.197	81.7

TABLE II
TABLE PRESENTING SV-NET PERFORMANCE UNDER VISUAL AND DYNAMIC DISTURBANCES.

A. Policy Architecture Ablations

We evaluated our main policy versus three ablations on a 15-second trajectory that guides the drone through a gate and under a ladder before ending facing a monitor. The desired trajectory is visualized in the GSplat in Fig. 5, along with flights from each policy ablation. All policies were trained on the same expert MPC dataset using PyTorch, the Adam optimizer (learning rate $1e-4$), for approximately 12 hours on a desktop machine (i9-13900K, RTX 4090, 64GB RAM). The policy ablations are:

- **SV-Net:** Our proposed architecture with a locked pre-trained RMA network and 2nd-to-last layer latent code to the command network.
- **SV no RMA:** A minimal variant comprising only the feature extractor and command network. This serves as our closest approximation to a zero-shot equivalent of the few-shot policy described in [14].
- **SV no pre-train:** A variant of SV-Net that skips the RMA network pre-training and goes directly to training the entire network (with the history network unlocked).
- **SV no latent:** Same as SV-Net, but uses the RMA’s explicit estimate of θ instead of the 2nd-to-last layer.

As shown in Table I, we found that **SV-Net** outperformed all other architectures, achieving a success rate of 100% and a trajectory tracking error of 0.173m, more than doubling the performance of **SV no RMA**. Pre-training the history network proved essential because (we hypothesize) it allows the network to adapt to significant changes in the flight dynamics due to rotor effects close to obstacles and due to significant effects from battery drain throughout a trajectory and across multiple trajectories. Also, we suspect that using the 2nd-to-last layer instead of the last layer of the history network enhances performance as the higher dimensionality of the latent code outweighs the minimal information loss from excluding the final layer. Lastly we observe, albeit anecdotally, that when training on significantly larger datasets, **SV no pre-train**’s performance in trajectory tracking converges with **SV-Net** when tested within FiGS. However, at this scale, the associated training times become impractical.

B. Robustness Experiments

We execute the same SV-Net policy as in Section VI-A across five experiments, each introducing distinct disturbances, as shown in Fig. 6:

- **Lighting:** Scene brightness was reduced to 40% of original lumens.
- **Dynamic:** Four people moved dynamically within the field of view along the trajectory.
- **Static:** The gate, ladder, and monitor (present at train time) were removed at runtime while the pillars adjacent to the gate were occluded.
- **Payload:** A rigid 350g payload (30% increase in drone weight) was attached.
- **Wind:** The drone was exposed to a 40 m/s wind gust using a leaf blower.

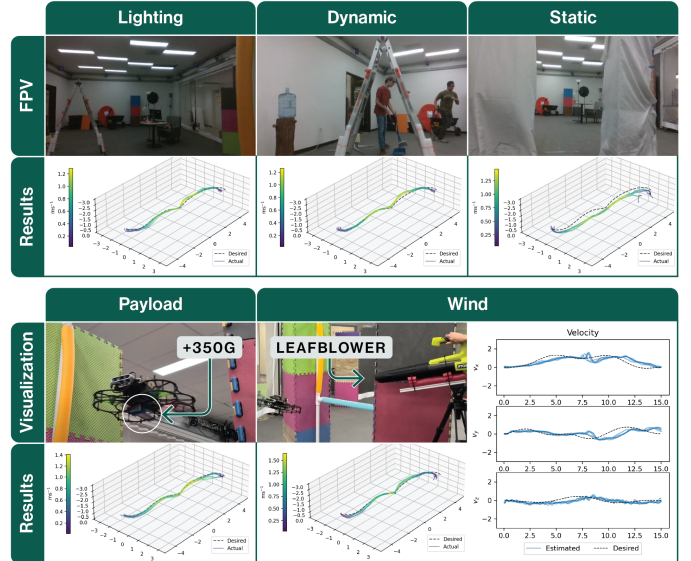


Fig. 6. Visualization of disturbances and the corresponding position and velocity performance of SV-Net. Lighting: illumination reduced by 60%, Dynamic: people moving erratically in the scene, Static: objects from training removed or occluded at runtime, Payload: 30% increase in mass, Wind: 40 m/s gust from leaf blower. SV-Net maintains adequate performance in all cases.

The results in Table II show SV-Net consistently demonstrated resilience to dynamic disturbances, payload variations,

Scenario	Success		Partial Success	Failure		Collision Rate (hits/m)	Trajectory Tracking Error (m)	Proximity Percentile (%)
	No Collisions	Recovery		No Recovery	Off-Course			
Multi-Objective	15	0	0	0	0	0.00	0.203	83.4
Extended Trajectory	23	4	0	3	0	0.02	0.241	72.5
Cluttered Environment	13	1	0	0	1	0.01	n/a	n/a

TABLE III
TABLE SHOWCASING THE PERFORMANCE OF SV-NET ACROSS THREE DIFFERENT SKILLS.

and wind gusts, maintaining near-baseline performance with only marginal increases in trajectory tracking error. However, lighting changes led to partial failures under extremely low lumens, where distinguishing objects, such as a black monitor blending into the dim background, became challenging. We also note that when lighting dropped below 40% of the original lumens, the policy consistently failed by drifting off-course from the start location. Static scene changes proved to be the most challenging: (i) the policy underflew waypoints and experienced minor collisions with the occluded pillars, (ii) the policy consistently flew through the space where the rungs of the ladder would have been. Despite these difficulties, the policy reliably tracked the overall trajectory shape, recovered from collisions, and successfully reached the final position in 4 out of 5 flights. These results suggest that the policy retains critical scene information that would otherwise have been removed in approaches relying on visual abstractions.

C. Skill-Testing Experiments

In our last set of experiments, we trained three different SV-Net policies, one for each of the following scenarios:

- **Multi-Objective:** One policy was trained to execute three distinct trajectories within the same scene distinguished by unique objective inputs O^k (start and end points, and total trajectory time). Two trajectories used identical positional splines but traversing in opposite directions, while the third followed a climbing orbit.
- **Extended Trajectory:** The drone navigated a trajectory that is double the length and duration of the trajectory in previous sections.
- **Cluttered Environment:** The policy was deployed close to the ground in a highly cluttered workshop with obstacles spaced as close as 1.0 m apart. The workshop has no motion capture system, so no ground truth trajectory data is available. Instead, we visualize the flight using a time-lapse rendering.

Results are reported in Table III with illustration shown in Fig. 7. The multi-objective policy had mixed success, indicating the need for more robust objective encodings in future work. Though it achieved a 100% collision free success rate, we observed significant degradation in one of the three tasks, where the drone consistently under-flew the desired trajectory and over-shot its end point. In the extended trajectory, the policy performed comparably to shorter trajectories, maintaining low collision rates and a Proximity Percentile of 72.5% over 30 attempts. Finally, in the cluttered environment, the policy achieved a 93.3% success rate on a 25s trajectory in between tables in a visually complex environment, highlighting its robustness in practical applications without relying on external pose estimators. Since the environment lacked motion capture,

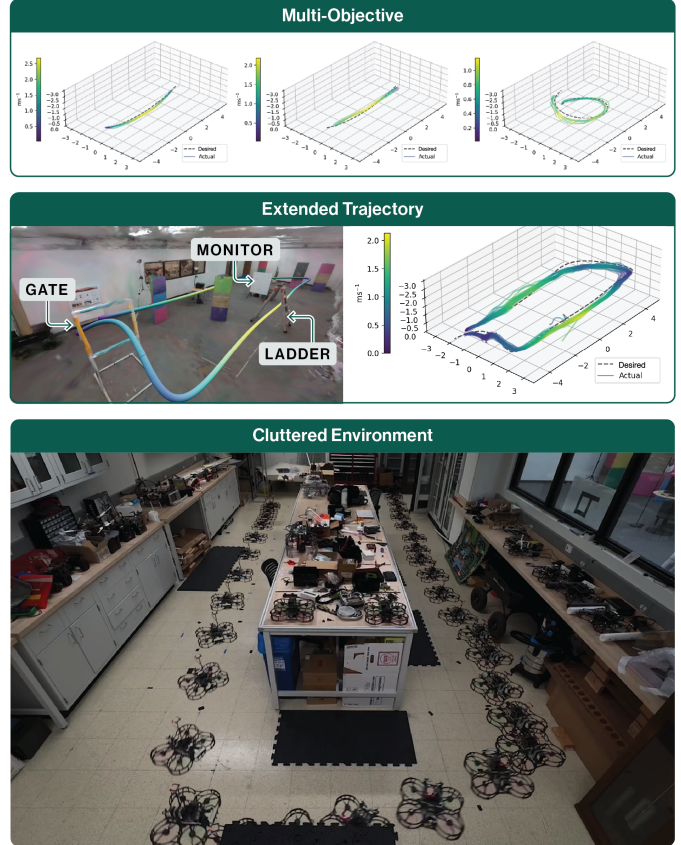


Fig. 7. 3D plots depicting performance of the skill-testing policies in Section VI-C. We show a time-lapse trajectory for the cluttered environment as this room does not have a motion capture system.

we cannot measure or report Trajectory Tracking Error or Proximity Percentile.

VII. CONCLUSIONS

This work introduces the SOUS VIDE approach for training end-to-end visual drone navigation policies. SOUS VIDE comprises the FiGS simulator based on a Gaussian Splatting scene model, data collection from an MPC expert, and distillation into a lightweight visuomotor policy architecture. By coupling high-fidelity visual data synthesis with online adaptation mechanisms, SOUS VIDE achieves zero-shot sim-to-real transfer, demonstrating robustness to variations in mass, thrust, lighting, and dynamic scene changes. Our experiments underscore the policy's ability to generalize across diverse scenarios, including complex and extended trajectories, with graceful degradation under extreme conditions. Notably, the integration of a streamlined adaptation module enables the policy to overcome limitations of prior visuomotor approaches, offering a computationally efficient yet effective solution for addressing model inaccuracies. These findings highlight the

potential of SOUS VIDE as a foundation for future advancements in autonomous drone navigation.

Limitations and Future Work: While its robustness and versatility are evident, challenges such as inconsistent performance in multi-objective tasks suggest opportunities for improvement through more sophisticated objective encodings. SOUS VIDE has been used to train policies that are highly optimized for a single real-life environment. Future work will explore training policies with the same tools across multiple environments in FiGS to enable generalist skills, like general collision avoidance, and scene-agnostic navigation. We will also explore augmenting SOUS VIDE policies with semantic goal understanding, so goals can be given by a human operator in the form of natural language commands. Ultimately, this work paves the way for deploying learned visuomotor policies in real-world applications, bridging the gap between simulation and practical autonomy in drone operations.

REFERENCES

- [1] A. Loquercio, E. Kaufmann, R. Ranftl, M. Müller, V. Koltun, and D. Scaramuzza, "Learning high-speed flight in the wild," *Science Robotics*, vol. 6, no. 59, p. eabg5810, 2021.
- [2] E. Kaufmann, L. Bauersfeld, A. Loquercio, M. Müller, V. Koltun, and D. Scaramuzza, "Champion-level drone racing using deep reinforcement learning," *Nature*, vol. 620, no. 7976, pp. 982–987, 2023.
- [3] I. Geles, L. Bauersfeld, A. Romero, J. Xing, and D. Scaramuzza, "Demonstrating agile flight from pixels without state estimation," in *Robotics: Science and Systems*, 2024.
- [4] B. Kerbl, G. Kopanas, T. Leimkühler, and G. Drettakis, "3d gaussian splatting for real-time radiance field rendering," *ACM Trans. Graph.*, vol. 42, no. 4, pp. 139–1, 2023.
- [5] M. Tancik, E. Weber, E. Ng, R. Li, B. Yi, J. Kerr, T. Wang, A. Kristoffersen, J. Austin, K. Salahi, A. Ahuja, D. McAllister, and A. Kanazawa, "Nerfstudio: A modular framework for neural radiance field development," in *ACM SIGGRAPH 2023 Conference Proceedings*, ser. SIGGRAPH '23, 2023.
- [6] S. Shah, D. Dey, C. Lovett, and A. Kapoor, "Airsim: High-fidelity visual and physical simulation for autonomous vehicles," in *Field and Service Robotics: Results of the 11th International Conference*. Springer, 2018, pp. 621–635.
- [7] W. Guerra, E. Tal, V. Murali, G. Ryou, and S. Karaman, "Flightgoggles: Photorealistic sensor simulation for perception-driven robotics using photogrammetry and virtual reality," in *2019 IEEE/RSJ International Conference on Intelligent Robots and Systems (IROS)*, 2019, pp. 6941–6948.
- [8] Y. Song, S. Naji, E. Kaufmann, A. Loquercio, and D. Scaramuzza, "Flightmare: A flexible quadrotor simulator," in *Conference on Robot Learning*. PMLR, 2021, pp. 1147–1157.
- [9] J. Panerati, H. Zheng, S. Zhou, J. Xu, A. Prorok, and A. P. Schoellig, "Learning to fly—a gym environment with pybullet physics for reinforcement learning of multi-agent quadcopter control," in *2021 IEEE/RSJ International Conference on Intelligent Robots and Systems (IROS)*, 2021, pp. 7512–7519.
- [10] M. Jacinto, J. Pinto, J. Patrikar, J. Keller, R. Cunha, S. Scherer, and A. Pascoal, "Pegasus simulator: An isaac sim framework for multiple aerial vehicles simulation," in *2024 International Conference on Unmanned Aircraft Systems (ICUAS)*, 2024, pp. 917–922.
- [11] B. Xu, F. Gao, C. Yu, R. Zhang, Y. Wu, and Y. Wang, "OmniDrones: An efficient and flexible platform for reinforcement learning in drone control," 2023.
- [12] F. N. Iandola, "Squeezenet: Alexnet-level accuracy with 50x fewer parameters and 0.5 mb model size," *arXiv preprint arXiv:1602.07360*, 2016.
- [13] A. Kumar, Z. Fu, D. Pathak, and J. Malik, "Rma: Rapid motor adaptation for legged robots," *arXiv preprint arXiv:2107.04034*, 2021.
- [14] A. Tagliabue and J. P. How, "Tube-nerf: Efficient imitation learning of visuomotor policies from mpc via tube-guided data augmentation and nerfs," *IEEE Robotics and Automation Letters*, 2024.
- [15] A. Quach, M. Chahine, A. Amini, R. Hasani, and D. Rus, "Gaussian splatting to real world flight navigation transfer with liquid networks," in *Proc. of the Conference on Robot Learning (CoRL)*, 2024.
- [16] A. Zhou, M. J. Kim, L. Wang, P. Florence, and C. Finn, "Nerf in the palm of your hand: Corrective augmentation for robotics via novel-view synthesis," in *Proceedings of the IEEE/CVF Conference on Computer Vision and Pattern Recognition*, 2023, pp. 17907–17917.
- [17] M. N. Qureshi, S. Garg, F. Yandun, D. Held, G. Kantor, and A. Silwal, "Splatsim: Zero-shot sim2real transfer of rgb manipulation policies using gaussian splatting," *arXiv preprint arXiv:2409.10161*, 2024.
- [18] T. Harnoja, B. Moran, G. Lever, S. H. Huang, D. Tirumala, J. Humplik, M. Wulfmeier, S. Tunyasuvunakool, N. Y. Siegel, R. Hafner *et al.*, "Learning agile soccer skills for a bipedal robot with deep reinforcement learning," *Science Robotics*, vol. 9, no. 89, p. eadi8022, 2024.
- [19] J. Tobin, R. Fong, A. Ray, J. Schneider, W. Zaremba, and P. Abbeel, "Domain randomization for transferring deep neural networks from simulation to the real world," in *2017 IEEE/RSJ International Conference on Intelligent Robots and Systems (IROS)*. IEEE, 2017, pp. 23–30.
- [20] G. M. Hoffmann, H. Huang, S. L. Waslander, and C. J. Tomlin, "Precision flight control for a multi-vehicle quadrotor helicopter testbed," *Control engineering practice*, vol. 19, no. 9, pp. 1023–1036, 2011.
- [21] M. Faessler, A. Franchi, and D. Scaramuzza, "Differential flatness of quadrotor dynamics subject to rotor drag for accurate tracking of high-speed trajectories," *IEEE Robotics and Automation Letters*, vol. 3, no. 2, pp. 620–626, 2017.
- [22] E. Tal and S. Karaman, "Accurate tracking of aggressive quadrotor trajectories using incremental nonlinear dynamic inversion and differential flatness," *IEEE Transactions on Control Systems Technology*, vol. 29, no. 3, pp. 1203–1218, 2020.
- [23] A. Bhattacharya, N. Rao, D. Parikh, P. Kunapuli, N. Matni, and V. Kumar, "Vision transformers for end-to-end vision-based quadrotor obstacle avoidance," *arXiv preprint arXiv:2405.10391*, 2024.
- [24] G. Loianno, C. Brunner, G. McGrath, and V. Kumar, "Estimation, control, and planning for aggressive flight with a small quadrotor with a single camera and imu," *IEEE Robotics and Automation Letters*, vol. 2, no. 2, pp. 404–411, 2016.
- [25] D. Zhang, A. Loquercio, X. Wu, A. Kumar, J. Malik, and M. W. Mueller, "Learning a single near-hover position controller for vastly different quadcopters," in *2023 IEEE International Conference on Robotics and Automation (ICRA)*. IEEE, 2023, pp. 1263–1269.
- [26] D. Zhang, A. Loquercio, J. Tang, T.-H. Wang, J. Malik, and M. W. Mueller, "A learning-based quadcopter controller with extreme adaptation," *arXiv preprint arXiv:2409.12949*, 2024.
- [27] S. Ross, N. Melik-Barkhudarov, K. S. Shankar, A. Wendel, D. Dey, J. A. Bagnell, and M. Hebert, "Learning monocular reactive uav control in cluttered natural environments," in *2013 IEEE international conference on robotics and automation*. IEEE, 2013, pp. 1765–1772.
- [28] F. Sadeghi and S. Levine, "Cad2rl: Real single-image flight without a single real image," *arXiv preprint arXiv:1611.04201*, 2016.
- [29] A. Loquercio, A. I. Maqueda, C. R. Del-Blanco, and D. Scaramuzza, "Dronet: Learning to fly by driving," *IEEE Robotics and Automation Letters*, vol. 3, no. 2, pp. 1088–1095, 2018.
- [30] D. Gandhi, L. Pinto, and A. Gupta, "Learning to fly by crashing," in *2017 IEEE/RSJ International Conference on Intelligent Robots and Systems (IROS)*. IEEE, 2017, pp. 3948–3955.
- [31] D. Shah, A. Sridhar, A. Bhorkar, N. Hirose, and S. Levine, "Gnm: A general navigation model to drive any robot," in *2023 IEEE International Conference on Robotics and Automation (ICRA)*. IEEE, 2023, pp. 7226–7233.
- [32] R. Doshi, H. Walke, O. Mees, S. Dasari, and S. Levine, "Scaling cross-embodied learning: One policy for manipulation, navigation, locomotion and aviation," *arXiv preprint arXiv:2408.11812*, 2024.
- [33] V. Ye, M. Turkulainen, and the Nerfstudio team, "gsplat." [Online]. Available: <https://github.com/nerfstudio-project/gspat>
- [34] R. Verschueren, G. Frison, D. Kouzoupis, J. Frey, N. van Duijkeren, A. Zanelli, B. Novoselnik, T. Albin, R. Quirynen, and M. Diehl, "acados – a modular open-source framework for fast embedded optimal control," *Mathematical Programming Computation*, 2021.
- [35] D. Mellinger and V. Kumar, "Minimum snap trajectory generation and control for quadrotors," in *2011 IEEE international conference on robotics and automation*. IEEE, 2011, pp. 2520–2525.
- [36] A. Tagliabue, D.-K. Kim, M. Everett, and J. P. How, "Efficient guided policy search via imitation of robot tube mpc," in *2022 International Conference on Robotics and Automation (ICRA)*. IEEE, 2022, pp. 462–468.
- [37] S. Ross, G. Gordon, and D. Bagnell, "A reduction of imitation learning and structured prediction to no-regret online learning," in *Proceedings of the fourteenth international conference on artificial intelligence and statistics*. JMLR Workshop and Conference Proceedings, 2011, pp. 627–635.